Palaeogeography, Palaeoclimatology, Palaeoecology 681 (2026) 113417

Contents lists available at ScienceDirect

Palaeogeography, Palaeoclimatology, Palaeoecology

journal homepage: www.elsevier.com/locate/palaeo

Ichnological analysis of the Paleocene Eocene thermal maximum

Sheridan Sigstad [a,*], Kurt O. Konhauser [a], Jens O. Herrle [b], Paul Myers [a], Alina Shchepetkina [c], Murray Gingras [a]

[a] Department of Earth and Atmospheric Sciences, University of Alberta, Edmonton, Alberta, Canada
[b] Institute of Geosciences, Goethe-University Frankfurt, Frankfurt, Germany
[c] Department of Earth Sciences, Western University, London, Ontario, Canada

ARTICLE INFO

Editor: L Angiolini

Keywords:
Paleocene-Eocene thermal maximum
Trace fossils
Ichnology
IODP expedition 392
Paleoenvironmental change
Benthic paleoecology

ABSTRACT

This study investigates the ichnological characteristics of deep-sea cores recovered from site U1580 on the southern Central Agulhas Plateau during International Ocean Discovery Program (IODP) Exp. 392, with a focus on the Paleocene-Eocene Thermal Maximum (PETM) event. By comparing pre-, *syn*-, and post-PETM intervals, this research applies trace fossil diversity, maximum trace diameter, and bioturbation patterns to assess benthic community responses to extreme climate changes including temperature changes, fluctuating bottom water oxygenation, nutrient availability, as well as changing deep sea circulation patterns. Trace fossil records such as ichnogenera diversity and maximum trace fossil diameters across 10 cm intervals (bins), were extracted from high-resolution photographs of cores U1580A and U1580B. Results reveal a reduction in maximum trace fossil diameters during the PETM, reflecting potential environmental stressors like elevated temperatures and lower oxygen (O_2) levels, followed by a post-PETM recovery. Trace fossil diversity increased from the *syn*- to post-PETM interval, ecological reorganization and potential recolonization of newly available niches. A comparative analysis of the two cores highlights subtle differences, with core U1580B exhibiting larger average maximum trace fossil diameters possibly due to localized variations in seafloor topography, food availability and/or biological factors. The deep-tier trace fossil *Zoophycos* is both included and excluded from the analysis to explore how its burrow depth – which likely exceeds the 10 cm bin intervals used – impacts ichnological trends. Overall, the ichnological patterns presented here provide new insights into how deep-sea macrobenthic communities responded to PETM environmental stressors, complementing existing paleoenvironmental interpretations based primarily on microfossil data.

1. Introduction

Approximately 55.9 million years ago, the PETM was marked by a rapid global temperature increase between 5 °C and 8 °C (Westerhold et al., 2009, 2017). As a result, sea surface temperatures rose by approximately 6 °C at high latitudes and 4 °C at low latitudes, while deepwater temperatures increased by around 8 °C at high latitudes and 6 °C at low latitudes (Kennett and Stott, 1991; Zachos et al., 2005; Jardine, 2011; Sluijs et al., 2011; Howard et al., 2025). This warming was accompanied by a pronounced negative shift in $\delta^{13}C$ values of approximately 3.5 ‰–4.5 ‰ at the onset of the PETM, driven by a geologically induced rapid release of carbon into the ocean-atmosphere system referred to as the Carbon Isotope Excursion (CIE; Kennett and Stott, 1991; Koch et al., 1992; Bralower et al., 1997; Zachos et al., 2005; McInerney and Wing, 2011).

The PETM introduced several interconnected stressors that reshaped marine ecosystems globally. Ocean stratification, driven by elevated temperatures, led to widespread anoxia in shallow- to intermediate-depth waters (< 2000 m; Kennett and Stott, 1991; Speijer and Wagner, 2002; Sluijs et al., 2008; Nicolo et al., 2010; Chun et al., 2010; Rodríguez-Tovar et al., 2011; Pälike et al., 2014; Sluijs et al., 2014; Zhou et al., 2016; Remmelzwaal et al., 2019), while deeper waters experienced only modest declines in seafloor O_2 levels (Chun et al., 2010; Pälike et al., 2014). Elevated atmospheric carbon dioxide (CO_2) levels caused substantial ocean acidification, reducing carbonate anion (CO_3^{2-}) availability and impairing calcification of marine organisms (Thomas, 1998, 2007; Penman et al., 2014; Kawahata et al., 2015; Schmidt et al., 2018). Concurrent alterations in the hydrological cycle— intensified weathering, precipitation, storm activity, and runoff—altered nutrient delivery to the oceans. Additionally, extreme temperatures imposed

* Corresponding author.
E-mail address: sigstad@ualberta.ca (S. Sigstad).

https://doi.org/10.1016/j.palaeo.2025.113417
Received 25 July 2025; Received in revised form 4 November 2025; Accepted 9 November 2025
Available online 10 November 2025

metabolic stress on marine life (Carmichael et al., 2017; Dossena et al., 2012; Lindmark et al., 2018). Deep-sea sedimentary records preserve these environmental perturbations. Through sedimentological, geochemical, and ichnological analyses, several studies have interpreted how elevated CO_2 levels, deoxygenation, and other stressors shaped marine ecological responses during the PETM (for example: Lu and Keller, 1993; Thomas and Shackleton, 1996; Alegret et al., 2009; Chun et al., 2010; Nicolo et al., 2010; Winguth et al., 2012; Sluijs et al., 2014; Nwojiji et al., 2023).

Among the many paleoenvironmental proxies available, ichnology—the study of trace fossils—provides direct evidence of past animal behaviors, including locomotion and feeding, as preserved in structures such as tracks and burrows (e.g., Schäfer, 1972; Ekdale et al., 1984; Bromley, 1996; Gingras et al., 2007; Seilacher, 2007). These traces, which record the effects of bioturbation, are extremely useful indicators of sedimentary conditions and animal responses to environmental stress (e.g., Bromley and Ekdale, 1984; Savrda and Bottjer, 1986, 1989, 1991; Gingras et al., 2007, 2011; Dashtgard, 2011; Savrda, 2007). The degree of bioturbation is commonly quantified using bioturbation index (BI) with an assigned value of 0 to 6. BI 0 is equivalent to no bioturbation observed and all original sedimentary structures preserved, whereas BI 6 means complete bioturbation with destruction of visible bedding (adapted and modified from Reineck, 1963; Taylor and Goldring, 1993). The presence, size and diversity of trace fossils, along with variations in bioturbation index, can reflect benthic ecosystem dynamics, nutrient cycling, and O_2 availability because trends in these data can be ascribed to environmental stresses (Pemberton et al., 1982; Savrda and Bottjer, 1986, 1989, 1991; Wetzel, 1991; MacEachern and Pemberton, 1992; Pemberton and Wightman, 1992; MacEachern et al., 2007; Wetzel, 2010; Rodríguez-Tovar, 2022). Despite the wealth of sediment core material recovered through the International Ocean Discovery Program (IODP)— over 98,000 m of core since 2013, with earlier programs dating back to 1968 (IODP Canada, 2024)—relatively little focus has been given to ichnological analyses of these archives. A missing piece of the puzzle of inestimable value for the reconstruction of the paleoenvironment of shallow to deep marine areas.

This study examines ichnological data in core material collected during IODP Expedition 392 (Uenzelmann-Neben et al., 2023), to enhance our understanding of how temperature, ocean circulation, and sedimentation patterns responded to fluctuations in CO_2 levels during the Cretaceous and Paleogene.

The primary objectives of this study were to use marine sediment core data as an archive to analyze ichnological characteristics across the PETM interval and to assess changes in trace fossil assemblages before, during, and after the event. By examining variations in trace fossil size and diversity, our study aims to reconstruct biological responses to environmental stress and infer shifts in bottom water and seafloor conditions. Although relatively few studies have considered ichnological responses to the PETM, notable studies by Nicolo et al. (2010), Rodríguez-Tovar et al. (2011), and Uchman et al. (2019) revealed a consistent pattern: an abrupt disappearance of visible trace fossils coinciding with the CIE, followed by the establishment of a low diversity assemblage dominated by very small (<1 mm) traces. Over time, ichnofossil diversity gradually recovered as larger and deeper-tier tracemakers reappeared. All three of these studies examined strata from paleowater depths of approximately 1000 to 2000 m. In contrast, this study focuses on a deeper marine setting (~2500 m paleodepth), providing a rare opportunity to explore macro-benthic community responses to extreme climate shifts in deeper ocean environments and to expand the currently limited ichnological record of the PETM.

2. Methods

Cores from site U1580 (holes A and B) were recovered between February 25th, 2022, and March 8th, 2022. Specific details on core recovery and handling can be found in the IODP Proceedings Volume 392 (Uenzelmann-Neben et al., 2023) and the Site U1580 summary (Bohaty et al., 2023). During this expedition, four drilling sites (U1579, U1580, U1581, and U1582) aimed to recover sedimentary records of the Paleocene-Eocene boundary. However, only site U1580 yielded suitable core material for ichnological analyses. Site U1580 was double-cored with U1580A (40°47.1535′S, 26°36.4137′E) and U1580B (40°47.1542′S, 26°36.4282′E) drilled ~20 m apart from each other. Located off the southern coast of Africa on the southern central Agulhas Plateau, this site lies at a modern water depth of 2560 m (Bohaty et al., 2023; Fig. 1). The Paleocene-Eocene boundary section was recovered from both cores and occurs at approximately 60 m below the seafloor. Paleo-water depth was likely similar to modern values or slightly shallower (Pérez-Díaz and Eagles, 2017).

For this study, high-resolution core photographs were obtained from the IODP online database (https://web.iodp.tamu.edu/OVERVIEW/). The downloaded images were enhanced using Affinity Designer 2 by adjusting levels to optimize contrast, improving the visibility of the sediment fabric and distinguishing trace fossils from the surrounding massive-appearing nannofossil clayey chalk (Fig. 2). The measurement tool in Affinity Designer 2 was calibrated using a 100 cm core section to ensure accurate measurements of trace fossil diameters.

Specific focus was placed on the cored intervals that span the PETM. This included 7.7 m of core from Hole U1580A (sections 7R1-7R6) and 4.9 m of core from Hole U1580B (sections 4R1-4R5) (Bohaty et al., 2023). The studied sections were subdivided into pre-, *syn*-, and post-PETM intervals (Table 1) with the syn-PETM interval being further separated into two sections: a clay-dominated syn-PETM (clay) at the onset of the PETM, followed by a slow recovery section syn-PETM (recovery). For cores U1580A and U1580B, pre-PETM values were obtained from 63.4-65.9 m (2.5 m) and 62.1–63.3 m (1.3 m) below sea floor, syn-PETM (clay) values were obtained from 62.7-63.3 m (0.6 m) and 61.5–62.1 m (0.6 m), syn-PETM (recovery) values were obtained from 61.3-62.6 m (1.3 m) and 60.1–61.4 m (1.3 m), and post-PETM values were obtained from 58.2-61.2 m (3.0 m) and 58.4–60 m (1.6 m), respectively. The amount of core used for pre- and post-PETM intervals was limited by missing core, while the syn-PETM (clay) intervals were constrained by magnetic susceptibility (MS) and natural gamma

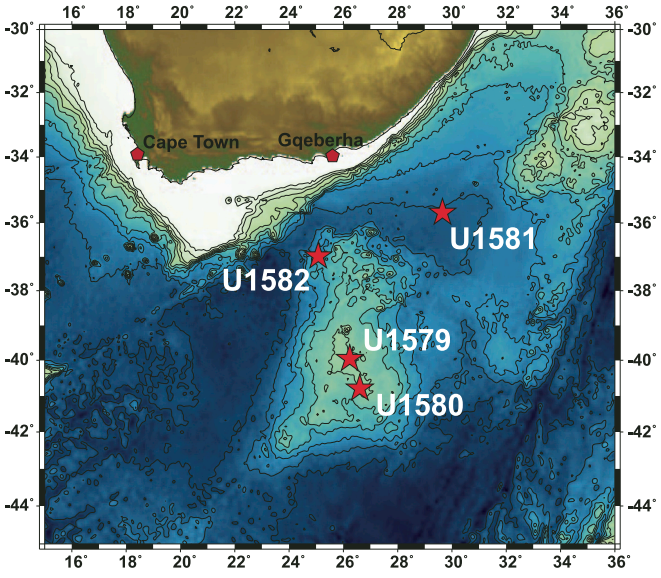

Fig. 1. IODP Expedition 392 site map from the southern coast of Africa (from IODP Proceedings Volume 392).

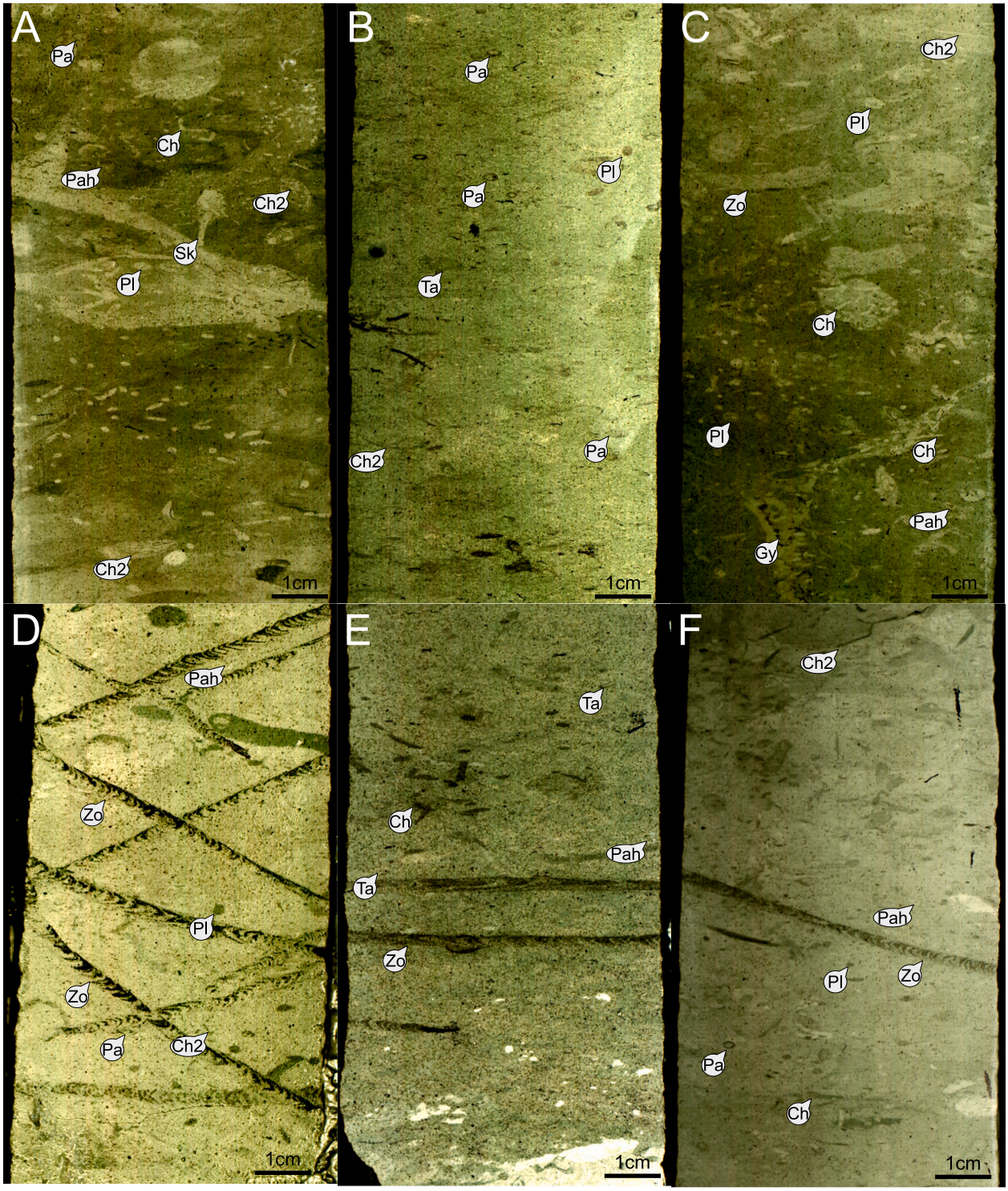

Fig. 2. U1580 core images. A) Core 1580A (~64 mbsf) showing the pre-PETM trace fossil assemblage. B) Core 1580A (~63.1 mbsf) showing the *syn*-PETM trace fossil assemblage with the PETM boundary located 13 cm below this image. C) Core U1580A (~60.5 mbsf) showing the post-PETM trace fossil assemblage. D) Core U1580B (~62.2 mbsf) showing the pre-PETM trace fossil assemblage. E) Core U1580B (~62 mbsf) showing the syn-PETM trace fossil assemblage with the PETM boundary located 1 cm below this image. Core U1580B (~59.2 mbsf) showing the post-PETM trace fossil assemblage. Ichnospecies presents include *Zoophycos* (Zo), *Chondrites* type 1 (Ch), *Chondrites* type 2 (Ch2), *Palaeophycus* sp. (Pa), *Palaeophycus heberti* (Pah), *Planolites* (Pl), *Taenidium* (Ta), and *Gyrolithes* (Gy).

ray (NGR) log trends in each core. Syn-PETM (recovery) intervals were constrained by MS along with statistical analyses on changing trace fossil diameters.

The onset of the PETM is evidenced in core by increased clay content with an abrupt change in sediment colour at a depth of ~63.3 m in U1580A and ~ 62.1 m in U1580B as well as the appearance of biohorizon base *Rhombaster* spp. (56.0 Ma) in core U1580A (63.38 m) (Zachos et al., 2005; John et al., 2012; Carmichael et al., 2017, IODP Proceedings Volume 392; Bohaty et al., 2023). For correlations, MS and NGR were used as proxies in lieu of any published $\delta^{13}C$ or $CaCO_3$ content analyses. Previous studies have shown that magnetic susceptibility correlates well with $CaCO_3$ trends, with a sharp increase at the start of

Table 1
PETM depth intervals for site U1580.

	1580A	1580B
Pre-PETM	63.4–65.9 m (2.5 m)	62.1–63.3 m (1.3 m)
Syn-PETM (clay)	62.7–63.3 m (0.6 m)	61.5–62.1 m (0.6 m)
Syn-PETM (recovery)	61.3–62.6 m (1.3 m)	60.1–61.4 m (1.3 m)
Post- PETM	58.2–61.2 m (3.0 m)	58.4–60 m (1.6 m)

the PETM event followed by a subsequent partial recovery that parallels $CaCO_3$ content (Stap et al., 2009). Similarly, NGR values have a sharp increase at the start of the PETM, followed by a gradual recovery to pre-PETM values, reflecting high clay content. These patterns were used to refine the placement of the *syn*-PETM interval in this study.

Core photos were divided into 10-cm bins, where the following characteristics were recorded for each bin: (1) ichnogenus (where possible) or trace fossil morphotype; (2) maximum diameter of trace fossils (causative tube) observed within each bin regardless of ichnogenera and specifically targeting the largest trace fossil observed within the 10-cm bin); and (3) ichnogenera diversity, defined as the total number of unique trace fossils observed withing the 10-cm bin. The diversity values were averaged within each PETM interval to emphasize shifts through time. Bioturbation index (BI) was not recorded because the studied core exhibits complete bioturbation (BI 6).

The average sedimentation rate of 1.79 cm/ka was calculated using the biohorizon base *Discoaster diastypus* (54.89 Ma) at a core depth of 43.66 m and the biohorizon base *Rhombaster* spp. (56.00 Ma) at a depth of 63.38 m in core U1580A, the same rate was also applied to core U1580B (IODP Proceedings Volume 392). This estimate assumes continuous and uniform sedimentation across the entire 19.72 m interval between both biohorizons– an assumption that is likely unrealistic. Hydrological changes during the PETM likely impacted sedimentation rates globally, and the presence of a 0.6 m clay layer at the onset of the PETM suggests a significant reduction in sedimentation rate—potentially <1 cm/ka—complicating PETM duration estimates (Röhl et al., 2007; Westerhold et al., 2018). Nevertheless, more precise constraints provided by micropaleontological data or cyclostratigraphic analysis are required to refine these estimates.

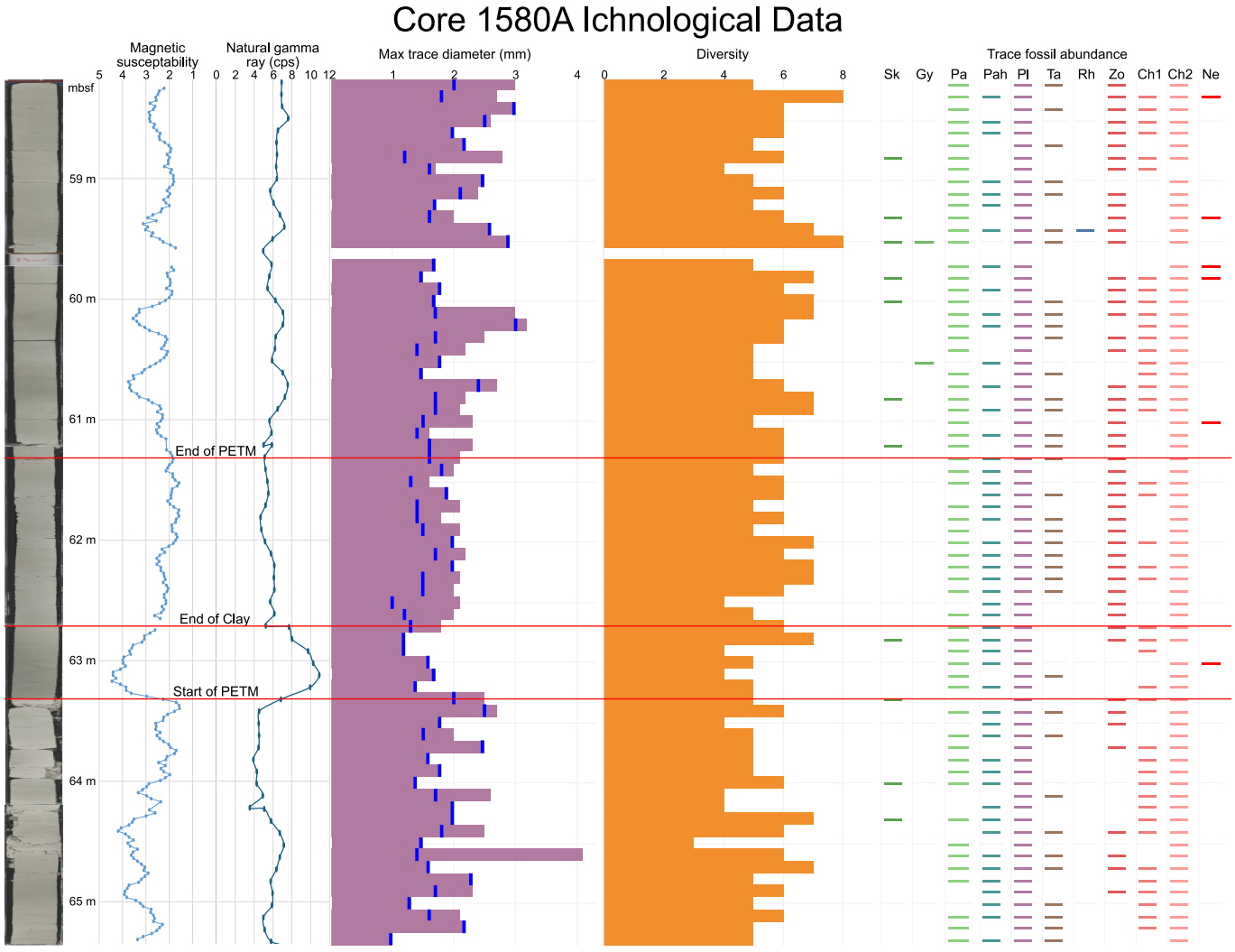

Fig. 3. Summary plot of ichnological data from core U1580A. From left to right: high-resolution core imagery, core depth in meters below the sea floor, magnetic susceptibility, gamma ray, maximum trace fossil diameter in millimeters, ichnodiversity, and ichnospecies identification. Maximum trace fossil diameter, ichnodiversity, and ichnospecies are recorded for each 10-cm interval. Maximum trace fossil diameter without *Zoophycos* is recorded by a vertical blue line for each 10-cm interval. The presence of at least one trace fossil of a given ichnospecies within the 10-cm interval is indicated by a colored horizontal dash. Ichnospecies present from left to right: *Skolithos* (Sk), *Gyrolithes* (Gy), *Palaeophycus* sp. (Pa), *Palaeophycus heberti* (Pah), *Planolites* (Pl), *Taenidium* (Ta), *Rhizocorallium* (Rh), *Zoophycos* (Zo), *Chondrites* Type 1 (Ch1), *Chondrites* Type 2 (Ch2), and *Nereities* (Ne). (For interpretation of the references to colour in this figure legend, the reader is referred to the web version of this article.)

3. Results

Data analyses were subdivided into four intervals: pre-PETM, *syn*-PETM (clay layer), syn-PETM (recovery), and post-PETM. Within each interval maximum trace fossil diameter, trace fossil diversity, and ichnogenera types, were recorded for each 10-cm bin. Figs. 3–5 illustrate these parameters for site U1580. Average maximum trace fossil diameters are summarized in Table 2.

Prior to the PETM, mean trace fossil diameters were 2.3 mm in core U1580A and 2.7 mm in core U1580B, with medians of 2.2 mm and 2.6 mm, maximum values of 4.1 mm and 4.0 mm, and minimum values of 1.0 mm and 1.3 mm, respectively. During the PETM clay interval, both cores show a reduction in maximum trace fossil diameters. In core U1580A, the mean diameter decreased to 1.5 mm, the median to 1.6 mm, the maximum to 1.8 mm, and the minimum to 2.6 mm. In core U1580B, the mean decreased to 2.1 mm, the mean to 2.3 mm, the maximum to 2.6 mm, and the minimum to 1.6 mm.

Following the clay interval, both cores show an increase in maximum trace fossil diameters during the recovery interval. In core U1580A, the mean and median diameters rise to 2.0 mm, with a maximum of 2.2 mm, and a minimum of 1.6 mm. In core U1580B, the mean and median increase to 2.3 mm, with a maximum of 3.0 mm and a minimum of 2.0 mm. Post-PETM, maximum trace fossil diameters continue to increase. In core U1580A, both the mean and median reach 2.3 mm, with a maximum of 3.2 mm and a minimum of 1.5 mm. In core U1580B, the mean and median reach 2.4 mm, with a maximum of 3.2 mm, and a minimum of 1.8 mm.

The trace fossil diversity values vary substantially across intervals, as summarized in Table 3. In the pre-PETM, the mean trace fossil diversity values are 5.3 for core U1580A and 5.2 for core U1580B, with medians of 5.0 in both cores. Maximum diversity reaches 7.0 in U1580A and 6.0 in U1580B, while minimum values are 3.0 and 4.0, respectively. During the *syn*-PETM clay interval, diversity declines slightly in both cores. Mean diversity decreases to 5.2 in U1580A and 5.0 in U1580B, while the median increases slightly to 5.5 in both. Maximum values remain unchanged at 7.0 and 6.0, and the minimum in both cores is 4.0.

In the syn-PETM recovery interval above the clay layer, average trace fossil diversity increases in both cores. Mean diversity rises to 5.8 in core U1580A and 6.0 in core U1580B, with median values of 6.0 in both. Maximum diversity reaches 7.0 in both cores, while minimum values are

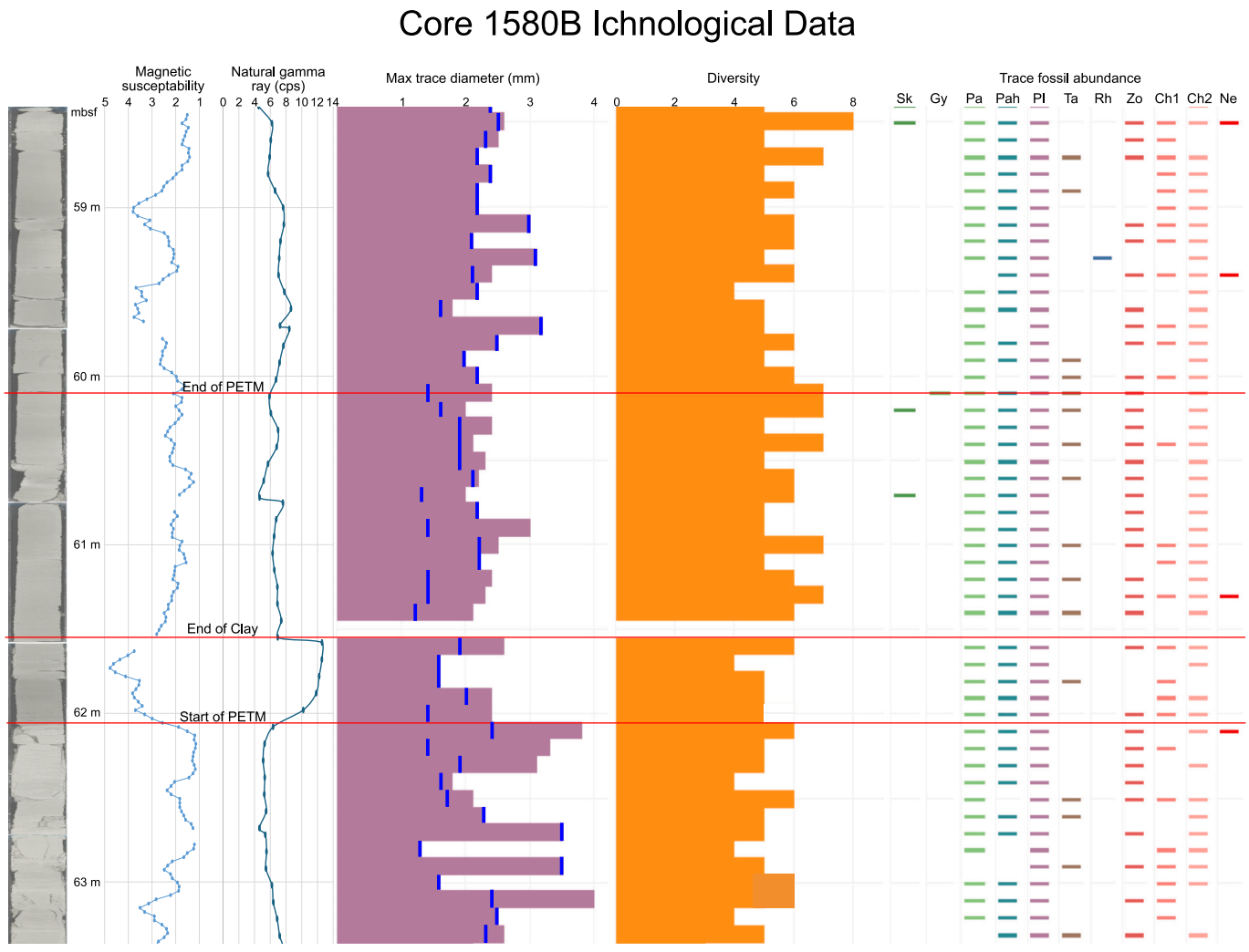

Fig. 4. Summary plot of ichnological data from core U1580B. From left to right: high-resolution core imagery, core depth in meters below the sea floor, magnetic susceptibility, gamma ray, maximum trace fossil diameter in millimeters, ichnodiversity, and ichnospecies identification. Maximum trace fossil diameter, ichnodiversity, and ichnospecies are recorded for each 10-cm interval. Maximum trace fossil diameter without *Zoophycos* is recorded by a vertical blue line for each 10-cm interval. The presence of at least one trace fossil of a given ichnospecies within the 10-cm interval is indicated by a colored horizontal dash. Ichnospecies present from left to right: *Skolithos* (Sk), *Gyrolithes* (Gy), *Palaeophycus* sp. (Pa), *Palaeophycus heberti* (Pah), *Planolites* (Pl), *Taenidium* (Ta), *Rhizocorallium* (Rh), *Zoophycos* (Zo), *Chondrites* Type 1 (Ch1), *Chondrites* Type 2 (Ch2), and *Nereities* (Ne). (For interpretation of the references to colour in this figure legend, the reader is referred to the web version of this article.)

Fig. 5. Box plots showing maximum trace fossil diameter and ichnodiversity for cores U1580A and U1580B with *Zoophycos* categorized into the pre-PETM, syn-PETM (clay), syn-PETM (recovery), and post-PETM intervals.

Table 2
Site U1580 summary statistics of maximum trace fossil diameter with *Zoophycos* separated into pre-PETM, syn-PETM (clay), syn-PETM (recovery), and post-PETM intervals.

Phase	1580A				1580B			
	Mean	Median	Max	Min	Mean	Median	Max	Min
Pre-PETM	2.3	2.2	4.1	1.0	2.7	2.6	4.0	1.3
Syn-PETM (Clay)	1.5	1.6	1.8	1.2	2.1	2.3	2.6	1.6
Syn-PETM (Recovery)	2.0	2.0	2.2	1.6	2.3	2.3	3.0	2.0
Post-PETM	2.3	2.3	3.2	1.5	2.4	2.4	3.2	1.8

Table 3
Site U1580 summary statistics for trace fossil diversity with *Zoophycos* separated into pre-PETM, syn-PETM (clay), syn-PETM (recovery), and post-PETM intervals.

Phase	1580A				1580B			
	Mean	Median	Max	Min	Mean	Median	Max	Min
Pre-PETM	5.3	5.0	7.0	3.0	5.2	5.0	6.0	4.0
Syn-PETM (Clay)	5.2	5.0	7.0	4.0	5.0	5.5	6.0	4.0
Syn-PETM (Recovery)	5.8	6.0	7.0	4.0	6.0	6.0	7.0	5.0
Post-PETM	6.0	6.0	8.0	4.0	5.6	5.0	8.0	4.0

4.0 in core U1580A and 5.0 in core U1580B. In the post-PETM interval, average diversity becomes more variable. In core U1580A, mean and median diversity increase to 6.0, with a maximum of 8.0 and a minimum of 4.0. In contrast, core U1580B shows a slight decrease in mean and median diversity to 5.6, with the same maximum (8.0) and minimum (4.0) values.

The most abundant trace fossils in both cores are *Planolites* (*Pl*), *Palaeophycus* sp. (*Pa*), and *Palaeophycus heberti* (*Pah*) (Saporta, 1872). *Chondrites* type 2 (*Ch2*) is also relatively common, followed by *Zoophycos* (*Zo*), and *Chondrites* type 1 (*Ch1*). Less frequently observed trace fossils include *Taenidium* (*Ta*), *Skolithos* (*Sk*), *Nereites* (*Ne*), *Gyrolithes* (*Gy*), *Phycosiphon* (*Ph*), *Spirophyton* (*Sp*), *Asterosoma* (*As*), and *Rhizocorallium* (*Rh*). *Chondrites* is classified into two types based on burrow diameter. Type 1 (*Ch1*) consists of branching tubes with diameters exceeding 0.5 mm, while Type 2 (*Ch2*) is characterized by smaller tubes, typically 0.1 to 0.3 mm in diameter. This distinction is crucial for interpreting bioturbation intensity and associated environmental conditions recorded in both cores. *Zoophycos*, which can extend to depths of up to 1 m, may reflect environmental signals from well above the sampled 10 cm intervals (Wetzel and Werner, 1980; Löwemark and Werner, 2001;

Löwemark and Grootes, 2004; Löwemark et al., 2004; Löwemark, 2007). Consequently, *Zoophycos* occurrences recorded may not accurately represent local environmental conditions during the PETM. To account for this, the adjusted dataset—excluding *Zoophycos*—is presented in Tables 4 and 5, with the implications of this adjustment discussed in detail later in this paper.

4. Interpretation and discussion

4.1. Trends in ichnological patterns

The analysis of ichnofossil abundance, maximum trace diameter, and diversity across the pre-, *syn*-, and post-PETM intervals reveals distinct patterns that shed light on past environmental conditions and biological responses. Prior to the PETM, average maximum trace fossil diameter were relatively large, reaching 2.3 mm in core U1580A and 2.6 mm in core U1580B. These values declined during the initial PETM clay interval to 1.5 mm and 2.1 mm, respectively—representing a 34.8 % decrease in U1580A and a 19.2 % decrease in U1580B. Diameters gradually increased during the recovery interval to 2.0 mm (U1580A) and 2.3 mm (U1580B), with further increases post-PETM to 2.3 mm and 2.4 mm, respectively. This represents a total increase of 53.3 % in U1580A and 14.3 % in U1580B relative to *syn*-PETM (clay) values.

Diminution in trace fossil size is a characteristic consequence of changing environmental stressors such as rising temperatures (Smith et al., 2009; Gingras et al., 2011; Rodríguez-Tovar, 2021), lowering O_2 levels (Savrda and Bottjer, 1986; Ekdale and Mason, 1988; Wignall and Hallam, 1991; Gingras et al., 1999; Savrda, 2007; Gingras et al., 2011) and changing salinity (Remane and Schlieper, 1972; Pemberton et al., 1982; Taylor and Goldring, 1993; Gingras et al., 1999; Gingras et al., 2011). Among these, the most likely stressor affecting deep-sea macrobenthic communities during the PETM was rising temperatures, which can directly influence animal body size by increasing metabolic demands. Dwarfing is a common physiological adaptation under such thermal stress (Smith et al., 2009; Garilli et al., 2015; Searing et al., 2023). Furthermore, as O_2 levels in the water column are reduced, animals will favor higher surface area-to-volume ratios, which is accomplished through body size reduction (Giere, 1993; Wetzel et al., 2001; Savrda, 2007).

Although changing salinity and ocean acidification are associated with the PETM, their direct impact on the macrobenthic community at site U1580 was likely minimal. Changing salinity levels can have a direct negative impact on trace fossil size and diversity in brackish water environments (Pemberton et al., 1982; MacEachern et al., 2007; Gingras et al., 2011) where salinity levels are significantly less than marine settings. However, estimates for PETM salinity changes are in the range of only 1–2 ppt (Harper et al., 2018), insufficient to drive significant ecological stress in deep-marine settings. Similarly, ocean acidification would have a large impact on organisms that require $CaCO_3$ to function (for instance corals, foraminifera, and any carbonate shell-producing organisms). However, these trace makers are largely confined to shallow- and intermediate-depth environments, whereas site U1580 was situated in deep water (~2500 m). Most tracemakers in this setting were likely soft-bodied vermiform invertebrates, which are not dependent on $CaCO_3$ structures and therefore less vulnerable to acidification. Thus, the observed reduction in trace fossil size at site U1580 during the PETM is best explained by elevated temperatures and resulting hypoxia, rather than salinity or pH changes.

The ichnodiversity exhibits notable temporal variation, with the lowest values recorded during the *syn*-PETM (clay) interval—5.2 in core U1580A and 5.0 in core U1580B. Diversity increases in the syn-PETM (recovery) interval to 5.8 and 6.0, respectively, and continues to rise post-PETM in core U1580A (6.0), while slightly decreasing in core U1580B (5.6). From the syn-PETM (clay) to post-PETM interval, this represents a total increase in ichnodiversity of 15.4 % in U1580A and 12.0 % in U1580B. Notably, both the recovery and post-PETM values surpass the pre-PETM diversity levels of 5.3 and 5.2, respectively. Trace fossil abundance also shift across the PETM interval. *Skolithos* and *Chondrites*, decline during the syn-PETM interval, and *Zoophycos* is absent for a 40 cm interval in U1580A and a 30 cm interval in U1580B beginning at the PETM onset. Conversely, the abundance of *Palaeophycus* sp., *Palaeophycus huberti*, and *Taenidium* increases. Notably, the post-PETM interval reveals a subsequent increase in *Skolithos*, *Chondrites*, and *Zoophycos* while the abundance of *Palaeophycus* sp., and *Taenidium* remains steady. This trend results in a rise in the trace fossil diversity during recovery and after the PETM event. The relatively stable ichnodiversity during the syn-PETM contrasts with previous ichnological studies, which typically report diversity loss associated with PETM conditions (Nicolo et al., 2010; Rodríguez-Tovar et al., 2011; Uchman et al., 2019). However, similar resilience has been observed in other benthic communities. For example, molluscan faunas and the shallow benthic communities in the Gulf Coastal Plain (USA) exhibited minimal PETM-related diversity loss and size reduction due to the warming event (Ivany et al., 2018; Foster et al., 2020). Ivany et al. (2018) specifically documented a temporary decrease in body size, followed by a rapid recovery and a slight increase in diversity during and after the PETM, consistent with the findings presented here.

The rise in trace fossil diversity may reflect the opportunistic colonization of new ecological niches in response to changing environmental conditions, such as global warming. It may also indicate a shift in behavioral strategies employed by the benthos (Nagelkerken and Munday, 2016; Buatois and Mángano, 2013, 2016; Buatois and Mángano, 2018). Given this context, trace fossil size may be a more diagnostic metric of environmental stress than ichnodiversity during times of warming.

Alternatively, changes in the direction and intensity of upwelling and downwelling currents during the PETM—discussed in more detail later—may have affected larval transport across the ocean floor, promoting opportunistic colonization (Bice and Marotzke, 2002; Tripati and Elderfield, 2005; Nunes and Norris, 2006). Many benthic invertebrates rely on specific current patterns for larval dispersal (Young et al., 2012; Cetina-Heredia et al., 2015; Hilário et al., 2015; Gary et al., 2020), and disruptions to these patterns could have altered dispersal trajectories, leading to settlement in novel habitats. The process of species migrating or expanding during warming events is well established in studies of foraminifera, plant species, and animals (Pross et al., 2012; Speijer et al., 2012; Giusberti et al., 2015).

It is also possible that the observed pattern of decreasing maximum trace fossil diameter coupled with increasing ichnofossil diversity reflects a scenario of reduced O_2 availability without a significant a

Table 4
Site U1580 summary statistics of maximum trace fossil diameter without *Zoophycos* separated into pre-PETM, syn-PETM (clay), syn-PETM (recovery), and post-PETM intervals.

Phase	1580A				1580B			
	Mean	Median	Max	Min	Mean	Median	Max	Min
Pre-PETM	1.9	1.7	3.2	1.0	2.2	2.3	3.5	1.3
Syn-PETM (Clay)	1.4	1.4	1.7	1.2	1.7	1.6	2.0	1.2
Syn-PETM (Recovery)	1.6	1.5	2.0	1.0	1.7	1.8	2.2	1.3
Post-PETM	2.0	1.8	3.0	1.2	2.3	2.2	3.2	1.6

Table 5
Site U1580 summary statistics for trace fossil diversity without *Zoophycos* separated into pre-PETM, syn-PETM (clay), syn-PETM (recovery), and post-PETM intervals.

Phase	1580A				1580B			
	Mean	Median	Max	Min	Mean	Median	Max	Min
Pre-PETM	4.9	5.0	7.0	3.0	4.4	4.0	5.0	3.0
Syn-PETM (Clay)	4.8	5.0	6.0	4.0	4.6	5.0	5.0	4.0
Syn-PETM (Recovery)	4.8	5.0	6.0	3.0	5.1	5.0	6.0	4.0
Post-PETM	5.1	5.0	7.0	3.0	5.0	5.0	7.0	4.0

corresponding decline in organic matter availability. This combination may account for the unexpected rise in trace fossil diversity despite dysoxic (i.e. low O_2) conditions. (Savrda and Bottjer, 1991; Wetzel and Uchman, 1998; Martin, 2003; Gingras et al., 2011). A decrease in oxygenation has been well established during the PETM (Lu and Keller, 1993; Thomas and Shackleton, 1996; Chun et al., 2010; Nicolo et al., 2010; Pälike et al., 2014; Remmelzwaal et al., 2019), yet the impact on nutrient dynamics and organic matter flux appears spatially variable and complex (Thomas et al., 2003; Alegret et al., 2009, 2021; Speijer et al., 2012; Winguth et al., 2012; Ma et al., 2014; Sluijs et al., 2014; Nwojiji et al., 2023). Evidence from other Southern Atlantic and Southern Ocean ODP sites (689, 690, 1262, 1263, 1265, 1267; Proceedings Volume 113 and 208) have reached similar conclusions. For instance, Alegret et al. (2021) investigated multiple ODP sites worldwide and reported that the absence of foraminiferal oligotrophic species *Nuttallides truempyi* might be linked to greater food supply in the Southern Ocean during the PETM. Similarly, Nwojiji et al. (2023) examined foraminifera from ODP site 1265A in the SE Atlantic Ocean (Walvis Ridge) and concluded that during the recovery interval of the CIE, the site experienced reduced O_2 stress and sustained nutrient/food supply, as indicated by the dominance of heavily calcified taxa.

Alegret et al. (2009) examined foraminiferal distribution and abundance in the Zumaya section (Spain) and found evidence of slightly lower O_2 levels but higher nutrient (and food) availability during the recovery interval of the CIE. However, these findings should not be interpreted as evidence that organic matter content and food availability remained constant everywhere during the PETM. On the contrary, multiple studies have documented reduced nutrient availability in other locations and at various oceanic depths (Rodríguez-Tovar et al., 2011; Winguth et al., 2012; Ma et al., 2014). Together, these examples underscore the complexity and variability of nutrient dispersal and accumulation during the PETM.

Given that our study area shows an increase in trace fossil diversity from the pre- to post-PETM intervals, and previous studies in the region indicate stable or high nutrient availability (Thomas et al., 2003; Alegret et al., 2009, 2021; Speijer et al., 2012; Nwojiji et al., 2023), we hypothesize that the observed reduction in trace fossil size represents an adaptive strategy to minimize O_2 demands, thus allowing organisms to conserve energy. Concurrently, steady nutrient availability allowed diversity to remain relatively stable.

4.1.1. Removal of Zoophycos from the dataset

Although ichnodiversity remains relatively stable throughout the PETM, suggesting a level of ecological resilience, a key consideration in interpreting the ichnological trends is the influence of large, deep-tier, trace fossils, such as *Zoophycos*. To ensure the accuracy of our ichnological interpretations, we examine the impact of *Zoophycos* on trace fossil size and diversity trends by comparing adjusted and unadjusted datasets.

Excluding *Zoophycos* notably reduces the maximum trace fossil diameter across all PETM intervals. Importantly, this adjustment improves the consistency between cores U1580A and U1580B, both of which then show a 0.5 mm decrease in maximum trace fossil diameter during the PETM, followed by a 0.6 mm increase by the post-PETM interval, ultimately surpassing pre-PETM averages (Tables 4 and 5). This convergence between cores, and the return to or exceeding of pre-PETM diameters in the post-event interval is significant, as it suggests a recovery of environmental conditions suitable for larger-bodied macrofauna.

4.2. Comparative analysis between cores

A comparative analysis of cores U1580A and U1580B provides valuable insight into the variability of benthic community responses during the PETM. Although the cores were collected from locations only ~20 m apart, they exhibit notable differences. For instance, core U1580A exhibits a noticeable increase in maximum trace fossil diameter from *syn*-PETM (clay) to the post-PETM, whereas core U1580B shows a more modest increase (+0.8 mm compared to +0.3 mm). Moreover, core U1580B exhibits a higher maximum trace fossil diameter across all intervals, averaging +0.35 mm greater than those observed in the corresponding intervals in U1580A. Trace fossil diversity is comparable between both cores, with a slight decline in diversity at the onset of the PETM, followed by a recovery in diversity that exceeds pre-PETM levels during the post-PETM interval. However, core U1580A displays a gradual change in trace fossil diversity across the intervals, whereas core U1580B reaches its peak diversity during the syn-PETM (recovery) interval. The recorded differences reflect spatial heterogeneity in deep-sea ichnofauna related to localized substrate conditions found on the Agulhas Plateau, such as ocean floor topography (e.g. sloped vs flat surfaces) and/or food availability. Notably, even minor changes in abyssal elevation changes—as little as 10 m—have been shown to influence megabenthic community structure, with reported variations of up to 10 % in community density and 59 % in biomass (Durden et al., 2020). Such fine-scale bathymetric variation may help explain the subtle but distinct differences in trace fossil size and diversity trends between the two closely spaced cores. Besides physical factors, biological factors may also have contributed to spatial heterogeneity, where ecological pressures are applied to minimize species competition, resulting in faunal segregation on the sea floor and patchiness on the substrate (Newell, 1979; Mángano et al., 2002; Veenma et al., 2025).

It is worth emphasizing that the observed patterns at site U1580—namely, a modest reduction in trace fossil size but an increase in ichnodiversity—are somewhat unexpected in light of previous PETM studies. Previous ichnological studies (e.g., Nicolo et al., 2010; Rodríguez-Tovar et al., 2011; Uchman et al., 2019) have generally reported a dramatic decline in trace fossil size and diversity, often approaching near-extinction levels, at the onset of the PETM. These reductions have typically been attributed to localized anoxia, followed by a protracted recovery interval.

In contrast, the ichnological record at site U1580 suggests a more resilient response to the PETM, or that PETM conditions were not as pronounced here as in other locations. While the moderate decrease in trace fossil size indicates environmental stress, the persistence of relatively high ichnodiversity implies sustained deep-sea oxygenation and that conditions never reached levels of severe anoxia. This raises important questions about the role of ocean circulation during the PETM and its influence on O_2 and organic matter delivery to Site U1580. These dynamics are further explored in the following section.

4.3. Ocean circulation and O_2 availability

Essential components for sustaining benthic life include the transport of food (organic matter) and oxygen from shallow/surface waters to deep ocean, primarily via processes such as oceanic downwelling and deep-water convection (Williams and Follows, 2003). In the absence of such transport, deep-sea O_2 levels can decline significantly, potentially leading to anoxic (i.e. absence of O_2) conditions that threaten the survival of benthic communities. At site U1580, both trace fossil diversity and maximum diameter decrease at the onset of the PETM, signaling environmental stress. However, the decline in diversity is modest, and there is no ichnological evidence for a significant reduction in the macrobenthic biomass. This pattern strongly suggests that, despite elevated temperatures and potential O_2 stress, the seafloor in the vicinity of the Agulhas Plateau continued to receive a steady supply of oxygenated and nutrient-rich waters throughout the PETM.

Several studies suggest that the PETM was marked by a major reorganization of deep-sea circulation, including a latitudinal shift in sites of oceanic downwelling—from Southern Ocean and South Atlantic to regions north of the equator in the Atlantic Ocean (Bice and Marotzke, 2002; Tripati and Elderfield, 2005; Nunes and Norris, 2006; Xue et al., 2023). This shift was likely driven by a reduced temperature gradient between the equator and poles, causing the ocean's overturning circulation to transition from primarily temperature-driven to salinity-driven processes (Kennett and Stott, 1991; Pak and Miller, 1992). Such a transition would be expected to weaken global overturning circulation, leading to stagnation of deep waters in the Southern Atlantic and promoting anoxic conditions. However, our ichnological data from Site U1580 show no evidence of such anoxia.

As deep waters age, they accumulate nutrients and isotopically light carbon (^{12}C), resulting in progressively more negative $\delta^{13}C$ values. This relationship allows the use of benthic foraminiferal carbon isotope records to trace deep-water formation and circulation patterns (Nunes and Norris, 2006). More negative $\delta^{13}C$ values indicate older, more nutrient-enriched waters, whereas more positive $\delta^{13}C$ values indicate younger waters near sites of deep-water formation (Nunes and Norris, 2006). During the PETM's CIE, evidence from $\delta^{13}C$ records indicates that deep-water formation occurred in the Atlantic Ocean north of the equator. At the same time, isotopically heavier (more positive) $\delta^{13}C$ values in the ancient Indian Ocean suggest that it also acted as a site of deep-water formation (Nunes and Norris, 2006). These younger, relatively well-oxygenated Indian Ocean deep waters appear to have flowed southward toward the tip of Africa—near the location of the present study—where they mixed with older, more δ^{12}-enriched waters, producing the intermediate $\delta^{13}C$ signatures observed in the region.

Despite proposed shifts in deep-water formation to the North Atlantic and Indian Ocean, some deep-water formation and associated O_2 transport likely continued within the Southern and South Atlantic basins, as supported by the similar neodymium (Nd) isotope signatures recorded from fossilized fish teeth across the North and South Atlantic, Southern Ocean, and ancient Indian Ocean (Thomas et al., 2003).

Consequently, site U1580 may have been uniquely positioned to receive contributions from multiple deep-water formation regions. In contrast, data from other Southern Ocean and South Atlantic Ocean ODP sites (e.g., Sites 689, 690, 738, 1262, 1263, and 1266; Proceedings Volumes 113, 119, and 208) show evidence of reduced oxygenation during the PETM, supported by elevated concentrations of redox-sensitive elements such as manganese (Mn) and uranium (U) in marine sediments and significant faunal turnover in benthic and planktonic foraminiferal assemblages that supports widespread ecological disruption (Lu and Keller, 1993; Thomas and Shackleton, 1996; Chun et al., 2010; Pälike et al., 2014).

However, detailed analyses of these sites indicate that suboxic conditions were generally confined to the CIE peak. At sites located below approximately 2500 m paleo-water depth (e.g., IODP sites 1262 and 1266 on the Walvis Ridge), oxic conditions appear to have resumed during the recovery phase of the CIE. This pattern suggests that while deep-ocean settings did experience some deoxygenation, they generally remained at least modestly oxygenated (i.e., suboxic) and were likely less affected by PETM-driven deoxygenation than shallower or intermediate-depth environments. In contrast, more severe anoxic conditions have been reported at shallower settings (Speijer and Wagner, 2002; Sluijs et al., 2008, 2014; Nicolo et al., 2010; Chun et al., 2010; Rodríguez-Tovar et al., 2011; Pälike et al., 2014).

The results of this study suggest that the sea floor at site U1580 was relatively unperturbed by the PETM warming event, with only a subtle decrease in maximum trace fossil diameters during the *syn*-PETM interval. Several scenarios may explain this limited response: (1) present downwelling models are likely too general in resolution to capture conditions at a single, geographically complex location on the sea floor, particularly one situated at the convergence of multiple oceanographic systems. Addressing this limitation would require additional ichnodiversity analyses from deep-sea cores across a broader range of global sites; (2) the macrobenthic community at U1580 may have experienced smaller shifts in O_2 availability than previously assumed, possibly due to a less extreme deoxygenation event on the sea floor; and (3) the site's position at the junction of the Southern Ocean, South Atlantic, and the ancient Indian Ocean likely exposed it to a dynamic mix of water masses and thermohaline circulation patterns. This complex setting may have enabled multiple O_2 delivery pathways, buffering the benthic community from more extreme conditions (a similar scenario from Uchman et al., 2019). Additionally, while circulation shifts likely influenced O_2 transport, the potential release of methane hydrates during the PETM—and their contribution to hypoxia—may also have played a role in shaping benthic ecosystem responses.

A major driver of PETM warming and the CIE was the relatively rapid release of large quantities of carbon into the atmosphere from various sources. These include the destabilization of methane hydrates on the seafloor (Dickens et al., 1995; Zachos et al., 2005), the thawing of permafrost (DeConto et al., 2012), and the release of thermogenic CH_4 and CO_2 from shallow marine volcanism in the North Atlantic (Svensen et al., 2004; Frieling et al., 2016; Berndt et al., 2023). Among these, the destabilization of methane hydrates is considered one of the most significant contributors, with estimates suggesting the release of approximately 2000–3000 Gt of isotopically light carbon ($\delta^{13}C \sim -60$ ‰), consistent with the magnitude and rapid onset of the CIE (Dickens et al., 1995; Dickens, 2011; Zachos et al., 2005).

The oxidation of methane (CH_4) in the water column consumes O_2 and produces CO_2. A rapid and large-scale release of methane hydrate would therefore have resulted in O_2-depleted waters. It is then plausible that these O_2-depleted waters could then have been transported via ocean currents and downwelling, allowing them to circulate along the seafloor and potentially impact benthic ecosystems far from the original methane release sites.

The decline in O_2 availability in seawater may partly account for the development of suboxic conditions at site U1580—as well as other Southern Ocean and Southern Atlantic sites— and contributed to the observed reduction in maximum trace fossil size during the syn-PETM interval. The substantial release of CH_4 into the oceans would have had a profound impact on ocean O_2 levels, with potentially profound consequences for the macrobenthic community. These findings underscore the need for further research into the role of CH_4 oxidation in shaping benthic ecosystem responses during the PETM. It is plausible that regions showing more extreme deoxygenation at the seafloor during the PETM may coincide with regions experiencing significant methane hydrate release (Nicolo et al., 2010; Pälike et al., 2014). As an example, Nicolo et al. (2010) studied a PETM-aged outcrop in New Zealand, originally deposited along the continental slope at upper to middle bathyal depths, and found a sharp decline in trace fossil abundance at the onset of the CIE, followed by a rapid recovery within ~50 ka. Using an O_2 box model, they demonstrated that the oxidation of a significant amount of released CH_4 could significantly amplify hypoxia: while

warming alone would have driven hypoxic conditions in ~23 % of intermediate waters, the addition of CH_4 oxidation increased this extent to ~59 %. These results strongly suggest that the oxidation of released CH_4 could have been a major contributor to mid-depth ocean hypoxia and the associated decline in macrobenthic activity, providing a compelling context to the patterns observed at Site U1580 (Nicolo et al., 2010). Accordingly, while these patterns remain inferential, we view the CH_4-oxidation–driven hypoxia mechanism as a working hypothesis; resolving the extent to which methane oxidation intensified deep ocean PETM deoxygenation will require targeted, cross-site, multi-proxy tests across basins before any firm causal claims can be made.

5. Conclusion

This study provides a comprehensive ichnological analysis, including trace fossil identification at the ichnogenera and ichnospecies levels, ichnodiversity, and maximum trace fossil diameter, in cores U1580A and U1580B. The cores were recovered during IODP Exp. 392, with a focus on the PETM. By evaluating trace fossil assemblages at both the ichnogenera and ichnospecies levels, as well as quantifying ichnodiversity and maximum trace fossil diameter, the study offers new insights into seafloor ecological dynamics during a period of rapid environmental change.

Key findings reveal a reduction in maximum trace fossil diameter during the syn-PETM interval, followed by a recovery in the post-PETM interval. Importantly, trace fossils did not disappear during the peak of the PETM, indicating that while benthic organisms were stressed, they remained active and capable of adapting. The post-PETM increase in ichnodiversity—exceeding pre-PETM levels in both cores—may reflect ecological niche expansion, adaptive behavioral shifts, and/or the persistence of organic matter availability that mitigated the effects of lowered oxygen levels and increased temperatures.

Comparative analysis between the two cores U1580A and U1580B, located ~20 m apart, highlights subtle but significant local variability—particularly a higher average maximum trace diameter in core U1580B, likely reflecting small-scale differences in seafloor topography, food supply and/or biological factors. The study also addresses the interpretive impact of deep-tier trace fossils, especially *Zoophycos*, whose exclusion from the dataset refines the signal of environmental change and clarifies the benthic response.

Overall, the ichnological stability observed at Site U1580 contrasts with more dramatic disruptions reported from other PETM records, underscoring the importance of regional context. The observed changes in trace fossil assemblages provide valuable insights into changing bottom water conditions, including water temperature, oxygenation, thermohaline circulation patterns, and nutrient availability. Unlike many prior studies that rely primarily on foraminiferal data, this study offers a macrofaunal perspective that broadens our understanding of marine ecosystem responses during the PETM. The findings emphasize the need for further ichnological studies from additional deep-sea sites to determine whether the patterns observed here are exceptional or more widespread. Ultimately, this research contributes critical palaeoecological data that enhances our understanding of deep-sea resilience and adaptation during one of Earth's most significant climate perturbations.

CRediT authorship contribution statement

Sheridan Sigstad: Writing – review & editing, Writing – original draft, Visualization, Methodology, Investigation, Formal analysis, Data curation, Conceptualization. **Kurt O. Konhauser:** Writing – review & editing. **Jens O. Herrle:** Writing – review & editing, Resources. **Paul Myers:** Writing – review & editing. **Alina Shchepetkina:** Writing – review & editing. **Murray Gingras:** Writing – review & editing, Validation, Supervision, Resources, Project administration, Methodology, Funding acquisition, Conceptualization.

Declaration of competing interest

The authors declare the following financial interests/personal relationships which may be considered as potential competing interests:

Murray Gingras reports financial support was provided by Natural Sciences and Engineering Research Council of Canada. If there are other authors, they declare that they have no known competing financial interests or personal relationships that could have appeared to influence the work reported in this paper.

Acknowledgements

We are grateful to the scientists and crew of IODP Expedition 392 for their efforts in collecting the core used in this study. Without such expeditions, research like this would not be possible. Additionally, we would like to thank all the authors for their insights and contributions. We gratefully acknowledge the support by NSERC Discovery Grant RGPIN-2020-0513 to MKG.

We thank Alfred Uchman and an anonymous reviewer for their constructive and thoughtful reviews, which helped to improve the quality of this manuscript.

Appendix A. Supplementary data

Supplementary data to this article can be found online at https://doi.org/10.1016/j.palaeo.2025.113417.

Data availability

Core data from IODP Expedition 392 are publicly available at the IODP database. Processed ichnological data generated during this study are available from the corresponding author upon request.

References

Alegret, L., Ortiz, S., Orue-Etxebarria, X., Bernaola, G., Baceta, J.I., Monechi, S., Apellaniz, E., Pujalte, V., 2009. The Paleocene Eocene Thermal Maximum: New Data on Microfossil Turnover at the Zumaia Section, vol. v. 24. PALAIOS, Spain, pp. 318–328. https://doi.org/10.2110/palo.2008.p08-057r.

Alegret, L., Arreguín-Rodríguez, G.J., Trasviña-Moreno, C.A., Thomas, E., 2021. Turnover and stability in the deep sea: benthic foraminifera as tracers of Paleogene global change. Glob. Planet. Chang. 196, 103372. https://doi.org/10.1016/j.gloplacha.2020.103372.

Berndt, C., Planke, S., Svensen, H., Millett, J.M., Tegner, C., Faleide, J.I., Callegaro, S., Kjøll, H.J., Frieling, J., Jones, M.T., Sluijs, A., 2023. Shallow-water hydrothermal venting linked to the Paleocene–Eocene Thermal Maximum. Nat. Geosci. 16, 803–809. https://doi.org/10.1038/s41561-023-01246-8.

Bice, K.L., Marotzke, J., 2002. Could changing ocean circulation have destabilized methane hydrate at the Paleocene/Eocene boundary? Paleoceanography 17, 1–8. https://doi.org/10.1029/2001PA000678.

Bohaty, S.M., Uenzelmann-Neben, G., Childress, L.B., Expedition 392 Scientists, 2023. Site u1580. In: Agulhas plateau cretaceous Climate, International Ocean Discovery Program, Proceedings of the International Ocean Discovery Program, 392. https://doi.org/10.14379/iodp.proc.392.2023.

Bralower, T.J., Thomas, D.J., Zachos, J.C., Hirschmann, M.M., Röhl, U., Sigurdsson, H., Thomas, E., 1997. High-resolution records of the late Paleocene thermal maximum and circum-Caribbean volcanism: is there a causal link? Geology 25 (11), 963–966. https://doi.org/10.1130/0091-7613(1997)025<0963:HRROTL>2.3.CO;2.

Bromley, R.G., 1996. Trace Fossils: Biology, Taxonomy and Applications, 2nd edition. Chapman and Hall, London, p. 361.

Bromley, R.G., Ekdale, A.A., 1984. Ichnology: The Use of Trace Fossils in Sedimentology and Stratigraphy: SEPM Short Course Notes, 15, p. 134.

Buatois, L.A., Mángano, M.G., 2013. Ichnodiversity and ichnodisparity: significance and caveats. Lethaia 46, 281–292. https://doi.org/10.1111/let.12018.

Buatois, L.A., Mángano, M.G., 2016. Recurrent patterns and processes: The significance of ichnology in evolutionary paleoecology. In: Mángano, M., Buatois, L. (Eds.), The Trace-Fossil Record of Major Evolutionary Events, vol. 40, pp. 449–473. https://doi.org/10.1007/978-94-017-9597-5_9. Topics in Geobiology.

Buatois, L.A., Mángano, M.G., 2018. The Trace-Fossil Record of Major Evolutionary Events v. 2: Mesozoic and Cenozoic. Topics in Geobiology, Vol. 41. Springer.

Carmichael, M.J., Inglis, G.N., Badger, M.P.S., Naafs, B.D.A., Behrooz, L., Remmelzwaal, S.R., Monteiro, F.M., Rohrssen, M., Farnsworth, A., Buss, H.L., Dickson, A.J., Valdes, P.J., Lunt, D.J., Pancost, R.D., 2017. Hydrological and associated biogeochemical consequences of rapid global warming during the

Paleocene Eocene thermal maximum. Glob. Planet. Chang. 157, 114–138. https://doi.org/10.1016/j.gloplacha.2017.07.014.
Cetina-Heredia, P., Roughan, M., van Sebille, E., Feng, M., Coleman, M.A., 2015. Strengthened currents override the effect of warming on lobster larval dispersal and survival. Glob. Chang. Biol. 21, 4377–4386. https://doi.org/10.1111/gcb.13063.
Chun, C.O., Delaney, M.L., Zachos, J.C., 2010. Paleoredox changes across the Paleocene Eocene thermal maximum, Walvis ridge (odp sites 1262, 1263, and 1266): evidence from Mn and U enrichment factors. Paleoceanography 25. https://doi.org/10.1029/2009PA001861.
Dashtgard, S.E., 2011. Linking invertebrate burrow distributions (neoichnology) to physicochemical stresses on a sandy tidal flat: Implications for the rock record. Sedimentology 58, 1303–1325.
DeConto, R.M., Galeotti, S., Pagani, M., Tracy, D., Schaefer, K., Zhang, T., Pollard, D., Beerling, D.J., 2012. Past extreme warming events linked to massive carbon release from thawing permafrost. Nature 484, 87–91. https://doi.org/10.1038/nature10929.
Dickens, G.R., 2011. Down the rabbit hole: toward appropriate discussion of methane release from gas hydrate systems during the Paleocene-Eocene thermal maximum and other past hyperthermal events. Clim. Past 7, 831–846. https://doi.org/10.5194/cp-7-831-2011.
Dickens, G.R., O'Neil, J.R., Rea, D.K., Owen, R.M., 1995. Dissociation of oceanic methane hydrate as a cause of the carbon isotope excursion at the end of the Paleocene. Paleoceanography v. 10, 965–971. https://doi.org/10.1029/95PA02087.
Dossena, M., Yvon-Durocher, G., Grey, J., Montoya, J.M., Perkins, D.M., Trimmer, M., Woodward, G., 2012. Warming alters community size structure and ecosystem functioning. Proc. R. Soc. B Biol. Sci. 279, 3011–3019. https://doi.org/10.1098/rspb.2012.0394.
Durden, J.M., Bett, B.J., Ruhl, H.A., 2020. Subtle variation in abyssal terrain induces significant change in benthic megafaunal abundance, diversity, and community structure. Prog. Oceanogr. 186, 102395. https://doi.org/10.1016/j.pocean.2020.102395.
Ekdale, A.A., Mason, T.R., 1988. Characteristic trace-fossil associations in oxygen-poor sedimentary environments. Geology 16, 720. https://doi.org/10.1130/0091-7613(1988)016<0720:CTFAIO>2.3.CO;2.
Ekdale, A.A., Bromley, R.G., Pemberton, S.G., 1984. Ichnology–the use of trace fossils in sedimentology and stratigraphy. In: Society of Economic Paleontologists and Mineralogists (Sepm), Short Course, 15, p. 317.
Foster, W.J., Garvie, C.L., Weiss, A.M., Muscente, A.D., Aberhan, M., Counts, J.W., Martindale, R.C., 2020. Resilience of marine invertebrate communities during the early Cenozoic hyperthermals. Sci. Rep. 10, 2176. https://doi.org/10.1038/s41598-020-58986-5.
Frieling, J., Svensen, H.H., Planke, S., Cramwinckel, M.J., Selnes, H., Sluijs, A., 2016. Thermogenic methane release as a cause for the long duration of the petm. Proc. Natl. Acad. Sci. 113, 12059–12064. https://doi.org/10.1073/pnas.1603348113.
Garilli, V., Rodolfo-Metalpa, R., Scuderi, D., Brusca, L., Parrinello, D., Rastrick, S.P.S., Foggo, A., Twitchett, R.J., Hall-Spencer, J.M., Milazzo, M., 2015. Physiological advantages of dwarfing in surviving extinctions in high-co2 oceans. Nat. Clim. Chang. 5, 678–682. https://doi.org/10.1038/nclimate2616.
Gary, S.F., Fox, A.D., Biastoch, A., Roberts, J.M., Cunningham, S.A., 2020. Larval behaviour, dispersal and population connectivity in the deep sea. Sci. Rep. 10, 10675. https://doi.org/10.1038/s41598-020-67503-7.
Giere, O., 1993. Meiobenthology. Springer, Berlin Heidelberg. https://doi.org/10.1007/978-3-662-02912-1.
Gingras, M.K., Pemberton, S.G., Saunders, T., Clifton, H.E., 1999. The ichnology of modern and Pleistocene brackish-water deposits at Willapa Bay, Washington: Variability in estuarine settings. PALAIOS 14, 352. https://doi.org/10.2307/3515462.
Gingras, M.K., Bann, K.L., MacEachern, J.A., Waldron, J., Pemberton, S.G., 2007. A conceptual framework for the application of trace fossils. In: MacEachern, J.A., Bann, K.L., Gingras, M.K., Pemberton, S.G. (Eds.), Applied Ichnology. SEPM Short Course Notes, pp. 1–26.
Gingras, M.K., MacEachern, J.A., Dashtgard, S.E., 2011. Process ichnology and the elucidation of physio-chemical stress. Sediment. Geol. 237, 115–134. https://doi.org/10.1016/j.sedgeo.2011.02.006.
Giusberti, L., Boscolo Galazzo, F., Thomas, E., 2015. Benthic foraminifera at the Paleocene/Eocene thermal maximum in the western Tethys (Forada section): Variability in climate and productivity. Clim. Past Discuss. 11, 4205–4245. https://doi.org/10.5194/cpd-11-4205-2015.
Harper, D.T., Zeebe, R., Hönisch, B., Schrader, C.D., Lourens, L.J., Zachos, J.C., 2018. Subtropical Sea-surface warming and increased salinity during Eocene thermal maximum 2. Geology 46, 187–190. https://doi.org/10.1130/G39658.1.
Hilário, A., Metaxas, A., Gaudron, S.M., Howell, K.L., Mercier, A., Mestre, N.C., Ross, R. E., Thurnherr, A.M., Young, C., 2015. Estimating dispersal distance in the deep sea: challenges and applications to marine reserves. Front. Mar. Sci. 2, 6. https://doi.org/10.3389/fmars.2015.00006.
Howard, C., Penman, D.E., Zhu, J., Harper, D.T., Newell, D.L., Norris, R.D., 2025. Tropical Atlantic temperature and hydrologic change during the Paleocene-Eocene thermal maximum. Paleoceanogr. Paleoclimatol. 40, e2024PA004939. https://doi.org/10.1029/2024PA004939.
Ivany, L.C., Pietsch, C., Handley, J.C., Lockwood, R., Allmon, W.D., Sessa, J.A., 2018. Little lasting impact of the Paleocene–Eocene thermal maximum on shallow marine molluscan faunas. Sci. Adv. 4, eaat5528. https://doi.org/10.1126/sciadv.aat5528.
Jardine, P., 2011. The Paleocene Eocene thermal maximum. Palaeontol. Online 1, 1–7. Article 5.
John, C.M., Banerjee, N.R., Longstaffe, F.J., Sica, C., Law, K.R., Zachos, J.C., 2012. Clay assemblage and oxygen isotopic constraints on the weathering response to the Paleocene Eocene thermal Maximum, east coast of North America. Geology 40, 591–594. https://doi.org/10.1130/G32785.1.
Kawahata, H., Nomura, R., Matsumoto, K., Nishi, H., 2015. Linkage of deep sea rapid acidification process and extinction of benthic foraminifera in the deep sea at the Paleocene/Eocene transition. Island Arc 24, 301–316. https://doi.org/10.1111/iar.12106.
Kennett, J.P., Stott, L.D., 1991. Abrupt deep-sea warming, palaeoceanographic changes and benthic extinctions at the end of the Paleocene. Nature 353, 225–229. https://doi.org/10.1038/353225a0.
Koch, P.L., Zachos, J.C., Dettman, D.L., 1992. Isotopic evidence for global climate change at the Paleocene–Eocene boundary. Nature 358, 319–322. https://doi.org/10.1038/358319a0.
Lindmark, M., Huss, M., Ohlberger, J., Gårdmark, A., 2018. Temperature-dependent body size effects determine population responses to climate warming. Ecol. Lett. 21, 181–189. https://doi.org/10.1111/ele.12880.
Löwemark, L., 2007. Importance and usefulness of trace fossils and bioturbation in paleoceanography. In: Miller, W. (Ed.), Trace Fossils. Elsevier, pp. 413–427. https://doi.org/10.1016/B978-044452949-7/50150-9.
Löwemark, L., Grootes, P.M., 2004. Large age differences between planktic foraminifers caused by abundance variations and Zoophycos bioturbation. Paleoceanography 19, PA1003. https://doi.org/10.1029/2003PA000949.
Löwemark, L., Werner, F., 2001. Dating errors in high-resolution stratigraphy: a detailed X-ray radiograph and AMS-14C study of Zoophycos burrows. Mar. Geol. 177, 191–198. https://doi.org/10.1016/S0025-3227(01)00167-0.
Löwemark, L., Chen, C.H., Huh, C.A., Lee, T.Q., Ku, Y.P., Yang, T.F., 2004. Biogenic reworking of tephra layers in the South China Sea (core md972142) and the Celebes Sea (core md012388). Ber. Sedimentol. 10, 7–13.
Lu, G., Keller, G., 1993. The Paleocene–Eocene transition in the Antarctic Indian ocean: Inference from planktic foraminifera. Mar. Micropaleontol. 21, 101–142. https://doi.org/10.1016/0377-8398(93)90012-M.
Ma, Z., Gray, E., Thomas, E., Murphy, B., Zachos, J., Paytan, A., 2014. Carbon sequestration during the Paleocene–Eocene thermal maximum by an efficient biological pump. Nat. Geosci. 7, 382–388. https://doi.org/10.1038/ngeo2139.
MacEachern, J.A., Pemberton, S.G., 1992. Ichnological aspects of cretaceous shoreface successions and shoreface variability in the western interior seaway of North America. In: Pemberton, S.G. (Ed.), Applications of Ichnology to Petroleum Exploration, A Core Workshop, 17, pp. 57–84. https://doi.org/10.2110/cor.92.17. SEPM Core Workshop.
MacEachern, J.A., Bann, K.L., Pemberton, S.G., Gingras, M.K., 2007. The ichnofacies paradigm: High-resolution paleoenvironmental interpretation of the rock record. In: MacEachern, J.A., Bann, K.L., Gingras, M.K., Pemberton, S.G. (Eds.), Applied Ichnology. SEPM Short Course Notes, 52, pp. 27–64. https://doi.org/10.2110/pec.07.52.0027.
Mángano, G.M., Buatois, L.A., West, R.R., Maples, C.G., 2002. Ichnology of a Pennsylvanian equatorial tidal flat—the stull shale member at Waverly, eastern Kansas. Kans. Geol. Surv. Bull. 245, 1–139.
Martin, R.E., 2003. The fossil record of biodiversity: Nutrients, productivity, habitat area and differential preservation. Lethaia 36, 179–194. https://doi.org/10.1080/00241160310005340.
McInerney, F.A., Wing, S.L., 2011. The Paleocene–Eocene thermal maximum: a perturbation of carbon cycle, climate, and biosphere with implications for the future. Annu. Rev. Earth Planet. Sci. 39, 489–516. https://doi.org/10.1146/annurev-earth-040610-133431.
Nagelkerken, I., Munday, P.L., 2016. Animal behaviour shapes the ecological effects of ocean acidification and warming: moving from individual to community-level responses. Glob. Chang. Biol. 22, 974–989. https://doi.org/10.1111/gcb.13167.
Newell, R.C., 1979. Biology of Intertidal Animals. Marine Ecological Surveys Ltd., Cape, p. 781.
Nicolo, M.J., Dickens, G.R., Hollis, C.J., 2010. South pacific intermediate water oxygen depletion at the onset of the Paleocene–Eocene thermal maximum as depicted in new Zealand margin sections. Paleoceanography 25. https://doi.org/10.1029/2009PA001904.
Nunes, F., Norris, R.D., 2006. Abrupt reversal in ocean overturning during the Paleocene/Eocene warm period. Nature 439, 60–63. https://doi.org/10.1038/nature04386.
Nwojiji, C., Marret, F., Caswell, B., Okoro, A.U., Igwe, E.O., 2023. Benthic foraminiferal turnover and trait changes across the Paleocene–Eocene thermal maximum (petm) at odp site 1265a, Walvis Ridge, SE Atlantic Ocean. Arab. J. Geosci. 16, 324. https://doi.org/10.1007/s12517-023-11417-x.
Pak, D.K., Miller, K.G., 1992. Paleocene to Eocene benthic foraminiferal isotopes and assemblages: Implications for Deepwater circulation. Paleoceanography 7, 405–422. https://doi.org/10.1029/92PA01234.
Pälike, C., Delaney, M.L., Zachos, J.C., 2014. Deep-sea redox across the Paleocene–Eocene thermal maximum. Geochem. Geophys. Geosyst. 15, 1038–1053. https://doi.org/10.1002/2013GC005074.
Pemberton, S.G., Wightman, D.M., 1992. Ichnological characteristics of brackish water deposits. In: Pemberton, S.G. (Ed.), Applications of Ichnology to Petroleum Exploration, A Core Workshop, 17, pp. 141–167. https://doi.org/10.2110/cor.92.17. SEPM Core Workshop.
Pemberton, S.G., Flach, P.D., Mossop, G.D., 1982. Trace fossils from the Athabasca oil Sands, Alberta, Canada. Science 217, 825–827. https://doi.org/10.1126/science.217.4562.825.
Penman, D.E., Hönisch, B., Zeebe, R.E., Thomas, E., Zachos, J.C., 2014. Rapid and sustained surface ocean acidification during the Paleocene–Eocene thermal maximum. Paleoceanography 29, 357–369. https://doi.org/10.1002/2014PA002621.

Pérez-Díaz, L., Eagles, G., 2017. South Atlantic paleobathymetry since early cretaceous. Sci. Rep. 7, 11819. https://doi.org/10.1038/s41598-017-11959-7.
Pross, J., Contreras, L., Bijl, P.K., Greenwood, D.R., Bohaty, S.M., Schouten, S., Bendle, J. A., Röhl, U., Tauxe, L., Raine, J.I., Huck, C.E., 2012. Persistent near-tropical warmth on the Antarctic continent during the early Eocene epoch. Nature 488, 73–77. https://doi.org/10.1038/nature11300.
Reineck, H.-E., 1963. Sedimentgefüge im Bereich der südlichen Nord-see. Abh Senckenberg Naturforsch Gesellschaft 505, 1–138.
Remane, A., Schlieper, C., 1972. Biology of Brackish Water, 2nd edition. wiley & Sons, p. 372. of 'die biologie des brackwassers'.
Remmelzwaal, S.R.C., Dixon, S., Parkinson, I.J., Schmidt, D.N., Monteiro, F.M., Sexton, P., Fehr, M.A., Peacock, C., Donnadieu, Y., James, R.H., 2019. Investigating ocean deoxygenation during the petm through the cr isotopic signature of foraminifera. Paleoceanogr. Paleoclimatol. 34, 917–929. https://doi.org/10.1029/2018PA003372.
Rodríguez-Tovar, F.J., 2021. Ichnology of the Toarcian oceanic anoxic event: an underestimated tool to assess palaeoenvironmental interpretations. Earth Sci. Rev. 216, 103579. https://doi.org/10.1016/j.earscirev.2021.103579.
Rodríguez-Tovar, F.J., 2022. Ichnological analysis: a tool to characterize deep-marine processes and sediments. Earth Sci. Rev. 228, 104014. https://doi.org/10.1016/j.earscirev.2022.104014.
Rodríguez-Tovar, F.J., Uchman, A., Alegret, L., Molina, E., 2011. Impact of the Paleocene–Eocene thermal maximum on the macrobenthic community: ichnological record from the Zumaia section, northern Spain. Mar. Geol. 282, 178–187. https://doi.org/10.1016/j.margeo.2011.02.009.
Röhl, U., Westerhold, T., Bralower, T.J., Zachos, J.C., 2007. On the duration of the Paleocene–Eocene thermal maximum (petm). Geochem. Geophys. Geosyst. 8, Q12002. https://doi.org/10.1029/2007GC001784.
Saporta, de G., 1872-1873. In: Masson, G. (Ed.), Paleontologie francaise ou description des fossiles de la France. 2 ser. Vegetaux. Plantes Jurassiques 1, 506.
Savrda, C.E., 2007. Trace fossils and benthic oxygenation. In: Miller III, W. (Ed.), Trace Fossils: Concepts, Problems, Prospects. Elsevier, pp. 149–158.
Savrda, C.E., Bottjer, D.J., 1986. Trace-fossil model for reconstruction of paleo-oxygenation in bottom waters. Geology 14, 3. https://doi.org/10.1130/0091-7613(1986)14<3:TMFROP>2.0.CO;2.
Savrda, C.E., Bottjer, D.J., 1989. Trace-fossil model for reconstructing oxygenation histories of ancient marine bottom waters: application to Upper cretaceous Niobrara Formation, Colorado. Palaeogeogr. Palaeoclimatol. Palaeoecol. 74, 49–74.
Savrda, C.E., Bottjer, D.J., 1991. Oxygen-related biofacies in marine strata: an overview and update. In: Tyson, R.V., Pearson, T.H. (Eds.), Modern and Ancient Continental Shelf Anoxia, 58, pp. 201–219. Geological Society of London, Special Publications.
Schäfer, W., 1972. Ecology and palaeoecology of marine environments. University of Chicago Press, Chicago, p. 568.
Schmidt, D.N., Thomas, E., Authier, E., Saunders, D., Ridgwell, A., 2018. Strategies in times of crisis—insights into the benthic foraminiferal record of the Paleocene–Eocene thermal maximum. Philos. Trans. R. Soc. A Math. Phys. Eng. Sci. 376, 20170328. https://doi.org/10.1098/rsta.2017.0328.
Searing, K.B., Lomolino, M.V., Rozzi, R., 2023. Melting climates shrink north American small mammals. In: Proceedings of the National Academy of Sciences, 120, e2310855120. https://doi.org/10.1073/pnas.2310855120.
Seilacher, A., 2007. Trace Fossil Analysis. Springer, Berlin, p. 226.
Sluijs, A., Röhl, U., Schouten, S., Brumsack, H.J., Sangiorgi, F., Sinninghe Damsté, J.S., Brinkhuis, H., 2008. Arctic late Paleocene–early Eocene paleoenvironments with special emphasis on the Paleocene–Eocene thermal maximum (Lomonosov Ridge, Integrated Ocean Drilling Program Expedition 302). Paleoceanography 23, PA1S11. https://doi.org/10.1029/2007PA001495.
Sluijs, A., Bijl, P.K., Schouten, S., Röhl, U., Reichart, G.-J., Brinkhuis, H., 2011. Southern ocean warming, sea level and hydrological change during the Paleocene–Eocene thermal maximum. Clim. Past 7, 47–61. https://doi.org/10.5194/cp-7-47-2011.
Sluijs, A., Van Roij, L., Harrington, G.J., Schouten, S., Sessa, J.A., LeVay, L.J., Reichart, G.-J., Slomp, C.P., 2014. Warming, euxinia and sea level rise during the Paleocene–Eocene thermal maximum on the gulf coastal plain: Implications for ocean oxygenation and nutrient cycling. Clim. Past 10, 1421–1439. https://doi.org/10.5194/cp-10-1421-2014.
Smith, J.J., Hasiotis, S.T., Kraus, M.J., Woody, D.T., 2009. Transient dwarfism of soil fauna during the Paleocene–Eocene thermal maximum. In: Proceedings of the National Academy of Sciences, 106, pp. 17655–17660. https://doi.org/10.1073/pnas.0909674106.
Speijer, R.P., Wagner, T., 2002. In: Renaut, R.W., Ashley, B.P. (Eds.), Sea-level changes and black shales associated with the Paleocene–Eocene thermal maximum: Implications for marine productivity and carbon burial, vol. v. 195, pp. 275–292. https://doi.org/10.1144/GSL.SP.2002.195.01.15. Geological Society, London, Special Publications.
Speijer, R.P., Scheibner, C., Stassen, P., Morsi, A.M.M., 2012. Response of marine ecosystems to deep-time global warming: A synthesis of biotic patterns across the Paleocene–Eocene Thermal Maximum (PETM). Austrian J. Earth Sci. 105, 6–16.
Stap, L., Sluijs, A., Thomas, E., Lourens, L., 2009. Patterns and magnitude of deep sea carbonate dissolution during Eocene thermal maximum 2 and h2, Walvis Ridge, southeastern Atlantic Ocean. Paleoceanography 24, PA1211. https://doi.org/10.1029/2008PA001655.
Svensen, H., Planke, S., Malthe-Sørenssen, A., Jamtveit, B., Myklebust, R., Rasmussen Eidem, T., Rey, S.S., 2004. Release of methane from a volcanic basin as a mechanism for initial Eocene global warming. Nature 429, 542–545. https://doi.org/10.1038/nature02566.
Taylor, A.M., Goldring, R., 1993. Description and analysis of bioturbation and ichnofabric. J. Geol. Soc. Lond. 150, 141–148. https://doi.org/10.1144/gsjgs.150.1.0141.
Thomas, E., 1998. Biogeography of the late Paleocene benthic foraminiferal extinction. In: Aubry, M.-P., Lucas, S.G., Berggren, W.A. (Eds.), Late Paleocene–Early Eocene Biotic and Climatic Events in the Marine and Terrestrial Records. Columbia University Press, New York, pp. 214–243.
Thomas, E., 2007. Cenozoic mass extinctions in the deep sea: what perturbs the largest habitat on Earth?. In: Large Ecosystem Perturbations: Causes and Consequences. Geological Society of America. https://doi.org/10.1130/2007.2424(01.
Thomas, E., Shackleton, N.J., 1996. The Paleocene–eocene benthic foraminiferal extinction and stable isotope anomalies. Geol. Soc. Lond., Spec. Publ. 101, 401–441. https://doi.org/10.1144/GSL.SP.1996.101.01.20.
Thomas, D.J., Bralower, T.J., Jones, C.E., 2003. Neodymium isotopic reconstruction of late Paleocene–early Eocene thermohaline circulation. Earth Planet. Sci. Lett. 209, 309–322. https://doi.org/10.1016/S0012-821X(03)00096-7.
Tripati, A., Elderfield, H., 2005. Deep-sea temperature and circulation changes at the Paleocene–Eocene thermal maximum. Science 308, 1894–1898. https://doi.org/10.1126/science.1109202.
Uchman, A., Egger, H., Rodríguez-Tovar, F.J., 2019. Changes in the composition of trace fossil assemblages across the Paleocene–Eocene transition in the north-western Tethys (Unterberg section, Austria). Geol. Carpath. 70, 3–13. https://doi.org/10.2478/geoca-2019-0001.
Uenzelmann-Neben, G., Bohaty, S.M., Childress, L.B., Expedition 392 Scientists, 2023. Expedition 392 summary. In: Agulhas Plateau Cretaceous Climate. International Ocean Discovery Program, Proceedings of the International Ocean Discovery Program, 392. https://doi.org/10.14379/iodp.proc.392.2023.
Veenma, Y.P., Davies, N.S., Shillito, A.P., 2025. The ichnological optimum: Enhanced trace fossil diversity in the Cambrian offshore driven by ecology, sedimentation, and outcrop. J. Geol. Soc. Lond. https://doi.org/10.1144/jgs2024-220.
Westerhold, T., Röhl, U., McCarren, H.K., Zachos, J.C., 2009. Latest on the absolute age of the Paleocene–Eocene thermal maximum (petm): New insights from exact stratigraphic position of key ash layers +19 and −17. Earth Planet. Sci. Lett. 287, 412–419. https://doi.org/10.1016/j.epsl.2009.08.027.
Westerhold, T., Röhl, U., Frederichs, T., Agnini, C., Raffi, I., Zachos, J.C., Wilkens, R.H., 2017. Astronomical calibration of the geological time scale: closing the middle Eocene gap. Clim. Past 13, 1129–1152. https://doi.org/10.5194/cp-13-1129-2017.
Westerhold, T., Röhl, U., Wilkens, R.H., Gingerich, P.D., Clyde, W.C., Wing, S.L., Bowen, G.J., Kraus, M.J., 2018. Synchronizing early Eocene deep-sea and continental records – cyclostratigraphic age models for the bighorn basin coring project drill cores. Clim. Past 14, 303–319. https://doi.org/10.5194/cp-14-303-2018.
Wetzel, A., 1991. Ecologic interpretation of deep-sea trace fossil communities. Palaeogeogr. Palaeoclimatol. Palaeoecol. 85, 47–69. https://doi.org/10.1016/0031-0182(91)90025-M.
Wetzel, A., 2010. Deep-sea ichnology: Observations in modern sediments to interpret fossil counterparts. Acta Geol. Pol. 60, 125–138.
Wetzel, A., Uchman, A., 1998. Deep-sea benthic food content recorded by ichnofabrics: a conceptual model based on observations from Paleogene Flysch, Carpathians, Poland. PALAIOS 13, 533. https://doi.org/10.2307/3515345.
Wetzel, A., Werner, F., 1980. Morphology and ecological significance of Zoophycos in deep-sea sediments off nw Africa. Palaeogeogr. Palaeoclimatol. Palaeoecol. 32, 185–212. https://doi.org/10.1016/0031-0182(80)90040-1.
Wetzel, M.A., Fleeger, J.W., Powers, S.P., 2001. Effects of hypoxia and anoxia on meiofauna: A review with new data from the Gulf of Mexico. In: Rabalais, N.N., Turner, R.E. (Eds.), Coastal Hypoxia: Consequences for Living Resources and Ecosystems. American Geophysical Union, pp. 165–184.
Wignall, P.B., Hallam, A., 1991. Biofacies, stratigraphic distribution and depositional models of British onshore Jurassic black shales. Geol. Soc. Lond., Spec. Publ. 58, 291–309. https://doi.org/10.1144/GSL.SP.1991.058.01.19.
Williams, R.G., Follows, M.J., 2003. Physical transport of nutrients and the maintenance of biological production. In: Fasham, M.J.R. (Ed.), Ocean Biogeochemistry. Global Change — The IGBP Series (closed). Springer, Berlin, Heidelberg. https://doi.org/10.1007/978-3-642-55844-3_3.
Winguth, A.M.E., Thomas, E., Winguth, C., 2012. Global decline in ocean ventilation, oxygenation, and productivity during the Paleocene–Eocene thermal maximum: implications for the benthic extinction. Geology 40, 263–266. https://doi.org/10.1130/G32529.1.
Xue, P., Chang, L., Thomas, E., 2023. Abrupt northwest Atlantic deep-sea oxygenation decline preceded the Paleocene–Eocene thermal maximum. Earth Planet. Sci. Lett. 618, 118304. https://doi.org/10.1016/j.epsl.2023.118304.
Young, C.M., He, R., Emlet, R.B., Li, Y., Qian, H., Arellano, S.M., Van Gaest, A., Bennett, K.C., Wolf, M., Smart, T.I., Rice, M.E., 2012. Dispersal of deep-sea larvae from the intra-American seas: simulations of trajectories using ocean models. Integr. Comp. Biol. 52, 483–496. https://doi.org/10.1093/icb/ics090.
Zachos, J.C., Röhl, U., Schellenberg, S.A., Sluijs, A., Hodell, D.A., Kelly, D.C., Thomas, E., Nicolo, M., Raffi, I., Lourens, L.J., McCarren, H., 2005. Rapid acidification of the ocean during the Paleocene–Eocene thermal maximum. Science 308, 1611–1615. https://doi.org/10.1126/science.1109004.
Zhou, X., Thomas, E., Winguth, A.M.E., Ridgwell, A., Scher, H., Hoogakker, B.A.A., Rickaby, R.E.M., Lu, Z., 2016. Expanded oxygen minimum zones during the late Paleocene–early Eocene: Hints from multiproxy comparison and ocean modeling. Paleoceanography 31, 1532–1546. https://doi.org/10.1002/2016PA003020.